Evaluation of Conventional and Imaging MIMO OWC Systems Using Linear Array Design

Chedlia Ben Naila, *Member, IEEE*, Tetsuya Nakamura, Hiraku Okada, *Member, IEEE*, and Masaaki Katayama, *Senior Member, IEEE*

***Abstract*—Multiple-input-multiple-output (MIMO) optical wireless communication systems are potential candidates for high-speed data transmission in indoor environments. In this work, we present an experimental evaluation of two different MIMO systems, i.e., conventional-MIMO (c-MIMO) and imaging-MIMO (i-MIMO) in terms of design considerations. Both systems use the same transmitter configuration featuring a one-dimensional (light-emitting diode) LED transmitting array. On the receiver side, the c-MIMO system employs a similar one-dimensional receiving avalanche photodetector (APD)-based array, whereas the i-MIMO system uses a customized imaging camera-based receiver design. To assess the performance of the two systems, the channel matrix and the bit-error rate are calculated based on the experimental data. At distances shorter than 50 m, the proposed c-MIMO system demonstrates a good transmission performance, particularly when the maximum likelihood detection (MLD) technique is applied. Whereas, at long distances ranging from 40 m to 65 m, the proposed i-MIMO system can ensure an error-free transmission due to the efficient spatial separation between the emitted optical beams. Furthermore, the experimental results confirm that our systems have the potential for high data rates over longer distances in indoor environments.**

***Index Terms*—Imaging receiver, linear array, optical wireless communications, OWC, optical wireless MIMO.**

I. Introduction

OPTICAL wireless communication (OWC) is emerging as an attractive solution for indoor industrial wireless applications where radio frequency (RF)-based systems are not suitable due to the harsh nature of the industrial environment [1]. In fact, unlike their counter partners RF systems, OWC systems offer the potential of high security at the physical layer thanks to their spatially confined optical carriers as well as immunity against both electromagnetic interference and interception, thus ensuring better flexibility and reliability in such challenging environments [2]. Moreover, OWC systems usually do not require complex digital signal processing and take advantage of the license-free and interference-free optical spectrum [3].

Manuscript received 8 August 2022; revised 24 August 2022; accepted 27 August 2022. Date of publication 1 September 2022; date of current version 13 September 2022. This work was supported in part by the Joint Research of Chubu Electric Power Company and the IMaSS of Nagoya University. *(Corresponding author: Chedlia Ben Naila.)*

Chedlia Ben Naila, Hiraku Okada, and Masaaki Katayama are with the Institute of Materials and Systems for Sustainability, IMaSS of Nagoya University, Nagoya 464-8603, Japan (e-mail: bennaila@nagoya-u.jp; hiraku@m.ieice.org; katayama@nuee.nagoya-u.ac.jp).

Tetsuya Nakamura is with Hitachi Group Corporate, Kanagawa 244-0817, Japan (e-mail: tetsuya.nakamura.bj@hitachi.com).

Digital Object Identifier 10.1109/JPHOT.2022.3203424

Despite the conspicuous development of OWC-based systems in the last decade, there is still a need to improve communication performance to meet the ever-increasing demand for higher capacity. In indoor environments, achieving high-speed transmission over long distances can be challenging considering that the light-emitting diodes (LEDs) have larger beam divergence than the laser diodes, thus limiting the transmission distance. An interesting approach consists of employing a pervasive multiplexing method widely used in RF communication, the multiple-input multiple-output (MIMO), to increase the data rate and spectral efficiency.

The application of the conventional MIMO (c-MIMO) array configurations featuring multiple LEDs and photodetectors (PDs) have attracted much interest in the OWC field [4], [5], [6]. Most of the research studies [7], [8], [9], [10] have focused on evaluating communication over short distances. For instance, the authors in [7] reported the transmission of a 500 Mbps data rate using a 2×2 c-MIMO configuration over a short distance of 40 cm. In [8], a higher data rate of 1 Gbps was achieved over a link range of 1 m using a 3×3 c-MIMO array. On the other hand, a lower data rate communication of 16 Mbps over a 1 m distance and 50 Mbps over a distance of 2 m was shown in [9] and [10], respectively, while a 4×4 c-MIMO system was used.

In the aforementioned studies, high data rate transmission was only possible over a few meters short distances. In order to increase the communication range, after a successful attempt of 20 Mbps data rate transmission over 15 m [11], we could achieve a higher data rate of 100 Mbps communication at a long distance of 65 m [12]. Furthermore, at short distances, we showed that using our newly proposed linear arrangement for transmitting and receiving arrays could efficiently reduce the correlations between the different elements of the channel matrix [12]. However, at longer distances, the elements of the channel matrix become highly correlated, which leads to the deterioration of the system performance.

To tackle this problem, the imaging MIMO, referred to as i-MIMO, receivers have shown to be a viable solution considering their spatial resolution property [13], [14], [15], [16]. Furthermore, such a receiver design can efficiently alleviate the stringent requirement for an accurate alignment between transmitter and receiver. Several researchers have investigated the use of the i-MIMO systems [17], [18], [19]. The transmission of a data rate of 1 Gbps over a 1 m link has been presented in [18], whereas a data rate of 0.6 Gbps over 6 m has been

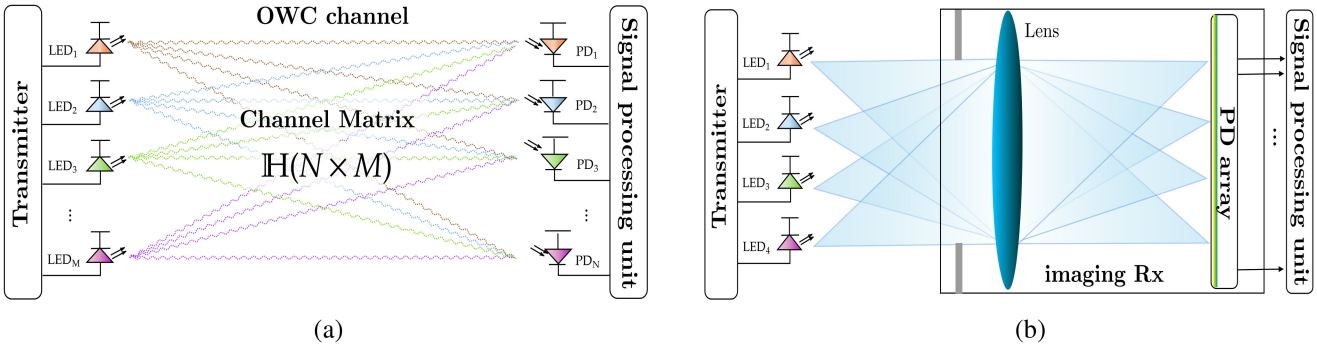

Fig. 1. General concept of (a) conventional MIMO-OWC system and (b) imaging MIMO receiver.

reported in [19]. Nonetheless, the majority of these studies were limited to analytical analyses [17], or experimental tests at short distances of less than 10 m [18], [19]. Our previous research work [20] presented an i-MIMO system featuring an improved design of an i-MIMO receiver that incorporates a telephoto lens placed in front of a classic single-lens reflex camera with a one-dimensional 16-element PD array. The transmitting array considered in [20] includes four optical emitting elements with an inter-element spacing of 25 cm. As a first experimental attempt, a transmission of a data rate of 100 Mbps for $4\times$ i-MIMO was obtained over 50 m [20].

In this paper, we report on two MIMO systems, c-MIMO and i-MIMO, that use the same transmitter configuration featuring a linear transmitting array with two different receivers. This new linear array is characterized by an eight-element array with a smaller inter-element spacing of 17.5 cm, capable of achieving a higher data rate transmission of 200 Mbps over a longer distance of 65 m. For the i-MIMO system, the same imaging receiver proposed in [20] is applied. We propose a comprehensive framework based on an experimental evaluation that captures the performance differences between conventional and imaging receiver configurations for MIMO systems while considering a new linear arrangement design for the optical arrays. The performance of the two developed systems is experimentally evaluated in terms of the bit-error rate and the channel matrix over a long link range up to 65 m.

The remainder of this paper is organized as follows. Section II details the configuration of the c-MIMO and i-MIMO systems. The conditions of the experimental tests are described in Section III. Section IV discusses the experimental performance results. Finally, the conclusion is provided in Section V.

II. System Configuration

In this work, we present two types of MIMO systems, c-MIMO, and i-MIMO, shown in Fig. 1(a) and (b), respectively, that exploit the new design of the linear element array presented in [12] and depicted in Fig. 2 while using different receiver configurations in an indoor environment.

For the c-MIMO system, we employ a receiver design including a one-dimensional receiving element array applying multiple photodetectors (APDs). In the i-MIMO system, we consider a customized imaging camera-based receiver design consisting of a telephoto lens placed in front of a linear APD array, as depicted in Fig. 3.

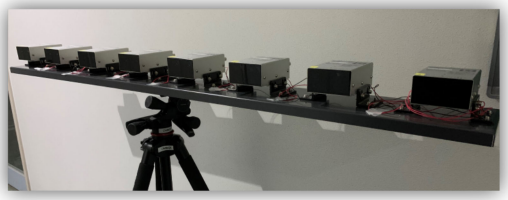

Fig. 2. Description of the eight-element array.

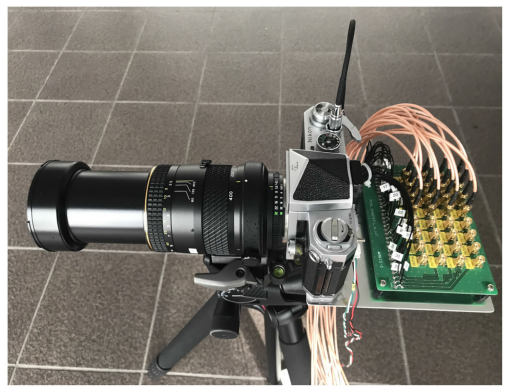

Fig. 3. Prototype of the imaging optical device.

A. Transmitter Design

As shown in Fig. 4(a), the transmitter structure includes three main parts, i.e., a transmitting signal processing unit, a digital-to-analog conversion (DAC) unit, and an optical transmitting unit.

1) Transmitting Signal Processing Unit: The input binary data stream is organized and formatted into identical frames with $\boldsymbol{d}_m[i] \in \{\pm 1\}$ being the i-th symbol in the frame of the m-th optical transmitting element.

Each transmitted data frame has a total length of $L_{fr} = 2600$ bits and consists of three distinct parts. The first part corresponds to a known preamble sequence of length $L_{pr} = 8$ bits and represented by $\boldsymbol{p} = [+1, -1, +1, -1, +1, -1, +1, -1]$. The

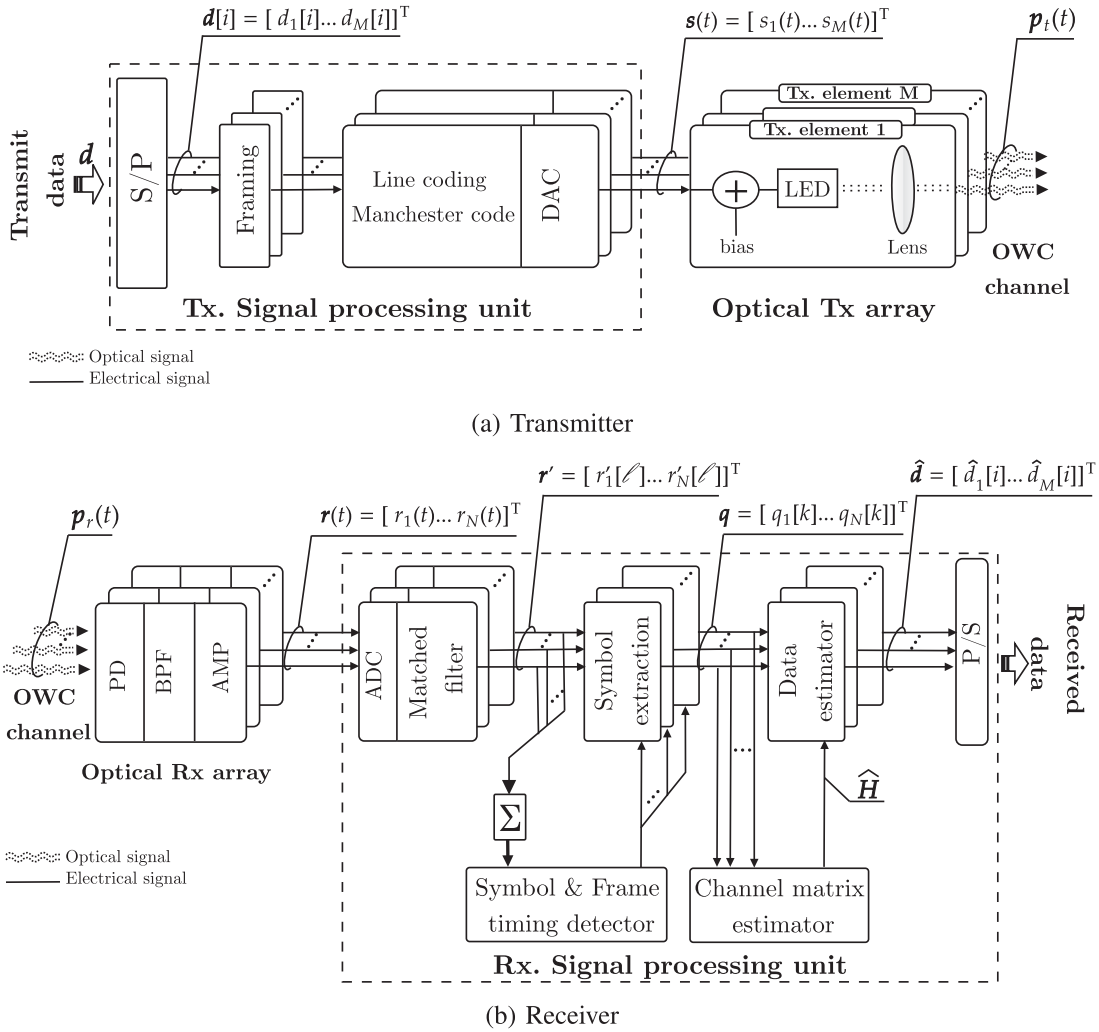

Fig. 4. Block diagrams of the transmitter and receiver.

same preamble, used in all the frames, is designed to identify the received symbol position and the start of the received frame. The second part contains a pilot denoted as $\boldsymbol{u_m}$ of length $L_p = 32$ bits and used for estimating the transmission channel matrix at the receiver. In this work, all the pilots $\boldsymbol{u_m}$ are orthogonal to each other. The third part of the data frame corresponds to a payload of length $L_{pa} = 2560$ bits.

The formatted data frames are encoded following Manchester coding technique at a symbol rate of $1/T_{\mathrm{Sym}}$ and then converted into electrical signals by the digital-to-analog converter (DAC).

The electrical signal to be input to the m-th optical transmitting element, $\boldsymbol{s}_m(t)$, can be represented as

$$\boldsymbol{s}_m(t) = \sum_{i=0}^{L_{\mathrm{fr}}-1} g(t - i\,T_{\mathrm{Sym}}) \cdot \boldsymbol{d}_m[i] \tag{1}$$

where $g(t)$ represents the Manchester-coded pulse defined as

$$g(t) = \begin{cases} +1 & (\text{if } -\frac{T_{\mathrm{S}}}{2} \le t < 0) \\ -1 & (\text{if } 0 < t \le \frac{T_{\mathrm{S}}}{2}) \\ 0 & \text{otherwise} \end{cases} \tag{2}$$

2) Optical Transmitting Unit: In [12], we proposed a new MIMO transmitter design featuring a one-dimensional optical array arrangement instead of the two-dimensional one. The performance tests have shown that such a configuration yields a significant performance enhancement compared to the square arrangement. In this work, we extend the application of this linear transmitting array with $M = 8$ transmitting elements, as shown in Fig. 2. Both c-MIMO and i-MIMO systems use the same transmitter configuration.

After being biased with a low direct current (DC), the electrical signal $\boldsymbol{s}_m(t)$ is modulated onto the optical power of the infrared LEDs and finally transmitted through the OWC channel.

The optical power $\boldsymbol{p}_{t,m}(t)$ generated from the signal $\boldsymbol{s}_m(t)$ is given by

$$\boldsymbol{p}_{t,m}(t) = P_0 \cdot \boldsymbol{s}_m(t) \tag{3}$$

where P_0 represents the incident optical power.

B. Receiver Design

This subsection presents the details of the signal process at the receiving side. As depicted in Fig. 4(b), the receiver structure is composed of three main parts, i.e., an optical receiving unit, an analog-to-digital conversion (ADC) unit, and a receiving signal processing unit. Note that the same processing is performed in the case of c-MIMO and i-MIMO receivers that we considered.

1) Optical Receiving Unit: In the c-MIMO system, the signals are directly received by multiple PDs and then processed to recover the transmitted data bits. Following the design concept introduced in [12], we considered a c-MIMO receiver that features a linear receiving array with N optical elements, similar to the transmitting array design ($N = M = 8$). On the other hand, in the i-MIMO system, a telephoto lens is placed in front of a classic single-lens reflex camera where the film has been replaced by a linear APD array ($N = 16$), as depicted in Fig. 3.

At the optical receiving unit, each optical power signal received by the n-th APD, $\boldsymbol{p}_{r,n}(t)$, is converted into an electrical signal after the elimination of the DC component, denoted as $\boldsymbol{r}_n(t)$.

2) Receiving Signal Processing Unit: The signal $\boldsymbol{r}_n(t)$ is sampled by the ADC at a period K of $T_{\rm spl}$ so that $T_{\rm Sym}/T_{\rm spl} = K$. The ADC output corresponding to the n-th APD, referred to as $\boldsymbol{r}_n[\ell]$, goes through the matched filter designed for the Manchester coding before being synchronized with an impulse response, $h[i]$, given by

$$h[i] = \begin{cases} -1 \ (0 \le i \le \frac{K}{2} - 1) \\ +1 \ (\frac{K}{2} - 1 < i \le K - 1) \end{cases} \tag{4}$$

The output signal of the n-th matched filter, $r'_n[\ell]$, can thus be expressed as

$$\boldsymbol{r}'_n[\ell] = \sum_{i=0}^{K-1} h[i]\boldsymbol{r}_n[\ell - i] \tag{5}$$

3) Synchronization: During the synchronization process, the detection of the symbol timing and the start of each frame is performed using the matched filter output at the time of the reception of the preamble $\boldsymbol{p}$ defined in Subsection II-A. Therefore, the correlation value between the matched filter output vector, $\boldsymbol{r'}_n^{(\ell)}$ for $KL_{\rm pr}$ samples and the preamble sequence $\boldsymbol{p}$ is maximized when ℓ coincides with the sample time at the start of the frame ℓ_0. The sample time at the beginning of the frame is obtained as follows:

$$\ell_0 = \arg\max_{\ell} \sum_{n=1}^{N} \boldsymbol{p}_{\rm c} \cdot \boldsymbol{r'}_n^{(\ell)} \tag{6}$$

where $\boldsymbol{r'}_n^{(\ell)}$, $\boldsymbol{p}_{\rm coded}$, and $\boldsymbol{M}$ are defined as follows

$$\begin{aligned} \boldsymbol{r'}_n^{(\ell)} &= [r'_n[\ell],\ r'_n[\ell+1],\ \cdots,\ r'_n[\ell + KL_{\rm pr} - 1]], \\ \boldsymbol{p}_{\rm c} &= [+\boldsymbol{M}, -\boldsymbol{M}, +\boldsymbol{M}, -\boldsymbol{M}, +\boldsymbol{M}, -\boldsymbol{M}, +\boldsymbol{M}, -\boldsymbol{M}], \\ \boldsymbol{M} &= [-1,\ -1,\ -1,\ -1,\ -1,\ +1,\ +1,\ +1,\ +1,\ +1]. \end{aligned}$$

Following the symbol synchronization, the matched filter output $\boldsymbol{r'}_n[\ell_0]$ is read every K samples. Let $q_n[k]$ denote the value of n-th APD symbol and given by

$$q_n[k] = \boldsymbol{r'}_n[\ell_0 - 1 + K \cdot k] \tag{7}$$

Thus, $q_{\rm n}[1] = \boldsymbol{r'}_n[\ell_0 + K]$ corresponds to the symbol marking the beginning of the frame.

4) Channel Matrix Estimation: After the symbol extraction step, it is possible to estimate the transmission channel matrix, $\boldsymbol{H}$, whose elements $h_{n,m}$ represent the propagation channel characteristics between the m-th optical transmitting element and the n-th receiving APD, and given by

$$\boldsymbol{H} = \begin{bmatrix} h_{1,1} & h_{1,2} & \dots & h_{1,M} \\ h_{2,1} & h_{2,2} & \dots & h_{2,M} \\ \vdots & \vdots & \vdots & \vdots \\ h_{N,1} & h_{N,2} & \dots & h_{N,M} \end{bmatrix} \tag{8}$$

Let $\boldsymbol{v}_n = [q_n[L_{pr}],\ q_n[L_{pr}+1],\ \cdots,\ q_n[(L_{pr}+L_p)-1]]$ denote the vector consisting of L_p received symbols corresponding to the pilot of the received frame of the n-th APD, considering the frame configuration described in Subsection II-A. $\boldsymbol{v}_n$ can be expressed based on the additive noise component N_n generated by the nth APD and the pilot $\boldsymbol{u}_m$ sent by the m-th optical transmitting element, as follows

$$\boldsymbol{v_n} = \sum_{m=1}^{M} h_{n,m}\boldsymbol{u_m} + \boldsymbol{N}_n \tag{9}$$

Since the vectors, $\boldsymbol{u}_m$ are orthogonal to each other, which means that

$$\boldsymbol{u}_m\boldsymbol{u}_{m'}^{\rm T} = \begin{cases} L_p \ (\text{if } m = m') \\ 0 \quad (\text{if } m \ne m') \end{cases} \tag{10}$$

Therefore, the estimate of the transmission channel matrix $\widehat{\boldsymbol{H}}$ of the aforementioned conventional and i-MIMO systems can be obtained as

$$\widehat{\boldsymbol{H}} = \frac{1}{L_p} \begin{bmatrix} \boldsymbol{v}_1 \\ \boldsymbol{v}_2 \\ \vdots \\ \boldsymbol{v}_N \end{bmatrix} \begin{bmatrix} \boldsymbol{u}_1^{\rm T} & \boldsymbol{u}_2^{\rm T} & \dots & \boldsymbol{u}_M^{\rm T} \end{bmatrix} \tag{11}$$

5) Data Estimation: Different detection algorithms are used in this work depending on the structure of the estimated channel matrix. For the i-MIMO system, we used the zero-forcing (ZF) technique which is particularly efficient in the noiseless channel. Whereas, for the c-MIMO system, we employed the maximum likelihood detection (MLD) as the transmission performance worsens for longer distances.

Considering the transmitted electrical signal vector $\boldsymbol{s}(t) = [\boldsymbol{s}_1(t), \boldsymbol{s}_2(t), \dots, \boldsymbol{s}_M(t)]^{\rm T}$, the corresponding received signal vector $\boldsymbol{r}(t) = [\boldsymbol{r}_1(t), \boldsymbol{r}_2(t), \dots, \boldsymbol{r}_M(t)]^{\rm T}$ can be expressed as

$$\boldsymbol{r}(t) = \boldsymbol{H}\boldsymbol{s}(t) + \boldsymbol{N}(t) \tag{12}$$

where $\boldsymbol{N}(t) = [N_1(t), N_2(t), \dots, N_N(t)]^{\rm T}$ is the real additive white Gaussian noise (AWGN) vector and $(\cdot)^{\rm T}$ denotes the transpose.

When the ZF technique is applied, the receiver produces an estimate of the transmitted vector, denoted as $\widehat{\boldsymbol{s}}(t)$, based on its

knowledge of the transmitted vector $\boldsymbol{s}(t)$, the channel matrix $\boldsymbol{H}$, and the observation $\boldsymbol{r}(t)$. $\widehat{\boldsymbol{s}}(t)$ can be described by

$$\begin{aligned}\widehat{\boldsymbol{s}}(t) &= \boldsymbol{H}^{+}\widehat{\boldsymbol{r}}(t)\\ &= \boldsymbol{s}(t) + \boldsymbol{H}^{+}\boldsymbol{N}(t)\end{aligned} \tag{13}$$

In the case of c-MIMO system $(N = M)$, $\widehat{\boldsymbol{H}}$ is a square invertible matrix and $\boldsymbol{H}^{+}$ corresponds to

$$\widehat{\boldsymbol{H}}^{+} = \widehat{\boldsymbol{H}}^{-1} \tag{14}$$

where $\boldsymbol{H}^{-1}$ is the inverse of the channel matrix $\widehat{\boldsymbol{H}}$.

In the case of i-MIMO system $(N > M)$, since $\boldsymbol{H}$ is a tall matrix and its inverse $\boldsymbol{H}^{-1}$ does not exist, it is possible to determine its pseudo-inverse instead. By applying the singular value decomposition (SVD), $\widehat{\boldsymbol{H}}$ can be written as [22]

$$\widehat{\boldsymbol{H}} = \boldsymbol{U}\boldsymbol{\Sigma}\boldsymbol{V} \tag{15}$$

where $\boldsymbol{U}$ and $\boldsymbol{V}$ represent $N \times N$ and $M \times M$ orthonormal matrices such that their columns include the left singular vectors and right singular vectors, respectively. $\boldsymbol{\Sigma}$ denotes a $N \times M$ tall matrix with zero-entries except for the singular values $[\sigma_1,\ \sigma_2,\ \cdots,\ \sigma_{M4pt}]$ appearing on the diagonal of its first M rows.

The pseudo inverse $\widehat{\boldsymbol{H}}^{+}$ can thus be computed using the inverse of its SVD as follows [22]

$$\widehat{\boldsymbol{H}}^{+} = \boldsymbol{V}\boldsymbol{\Sigma}^{+}\boldsymbol{U}^{\mathrm{T}} \tag{16}$$

where $\boldsymbol{\Sigma}^{+}_{M\times N4pt}$ represents the pseudo inverse of $\boldsymbol{\Sigma}_{N\times M4pt}$ with $[1/\sigma_1,\ 1/\sigma_2,\ \cdots,\ 1/\sigma_{M4pt}]$ on its diagonal and $\boldsymbol{U}^{\mathrm{T}}$ is the transpose of the matrix $\boldsymbol{U}$.

Considering the i-th transmitted data vector $\boldsymbol{d}[i]$, the corresponding received symbol vector $\boldsymbol{y}[i]$ can be expressed as

$$\boldsymbol{y}[i] = [q_1[L_p + i],\ q_2[L_p + i], \ldots,\ q_N[L_p + i]]^{\mathrm{T}} \tag{17}$$

The transmitted vector $\boldsymbol{x}[i] = [x_1[i],\ x_2[i], \ldots,\ x_M[i]]$, can be determined by multiplying $\widehat{\boldsymbol{H}}^{+}$ and the received symbol vector $\boldsymbol{y}[i]$, as follows

$$\boldsymbol{x}[i] = \widehat{\boldsymbol{H}}^{+}\boldsymbol{y}[i] \tag{18}$$

where $\widehat{\boldsymbol{H}}^{+}$ is given by (14) and (16) for c-MIMO system and i-MIMO system, respectively.

After the estimation and equalization of the channel matrix, the estimated value $\widehat{\boldsymbol{d}}_m[i]$ of the *i*-th symbol in the frame of the *m*-th optical transmitting element $\boldsymbol{d}_m[i]$ can be obtained as

$$\widehat{\boldsymbol{d}}_m[i] = \mathrm{sgn}(\boldsymbol{x}_m[i]) \qquad m = 1, 2, \ldots, M \tag{19}$$

where $\mathrm{sgn}(\cdot)$ represents the signum function.

To further improve the performance in the c-MIMO system, a more advanced detection based on the MLD algorithm is applied. As known, MLD offers an optimal detection, but at the cost of a prohibitive computational complexity [21].

Let $\boldsymbol{U}$ denote the set of possible values of the transmitted data vector $\boldsymbol{d}$. In this case, the estimated value $\widehat{\boldsymbol{d}}$ is given by

$$\begin{aligned}\widehat{\boldsymbol{d}} &= \arg\max_{\boldsymbol{d}\in\boldsymbol{U}} \mathrm{Prob}[\boldsymbol{d}|\boldsymbol{y}]\\ &= \arg\max_{\boldsymbol{d}\in\boldsymbol{U}} \mathrm{Prob}[\boldsymbol{y}|\boldsymbol{d}]\\ &= \arg\max_{\boldsymbol{d}\in\boldsymbol{U}} \mathrm{P}_{\boldsymbol{N}}(\boldsymbol{y} - \boldsymbol{H}\boldsymbol{d})\end{aligned} \tag{20}$$

where $P_{\boldsymbol{N}}(\cdot)$ represents the joint probability density function of the noise vector $\boldsymbol{N}$. Assuming that each element of $\boldsymbol{N}$ is independent of each other and follows a Gaussian distribution with zero mean and variance σ_n^2, then

$$\mathrm{P}_{\boldsymbol{N}}(N_1, N_2, \ldots, N_N) = \prod_{n=1}^{N} \frac{1}{\sigma_n\sqrt{2\pi}} \exp\left(-\frac{N_n^2}{2\sigma_n^2}\right) > 0 \tag{21}$$

By applying (21), (20) can be rewritten as

$$\begin{aligned}\widehat{\boldsymbol{d}} &= \arg\max_{\boldsymbol{d}\in\boldsymbol{U}} \ln \mathrm{P}_{\boldsymbol{N}}(\boldsymbol{y} - \boldsymbol{H}\boldsymbol{d})\\ &= \arg\max_{\boldsymbol{d}\in\boldsymbol{U}} \left[\ln\left(\prod_{n=1}^{N} \frac{1}{\sigma_n\sqrt{2\pi}}\right) - \sum_{n=1}^{N} \frac{(y_n - \boldsymbol{H}\boldsymbol{d})^2}{2\sigma_n^2}\right]\\ &= \arg\min_{\boldsymbol{d}\in\boldsymbol{U}} \sum_{n=1}^{N} \frac{(y_n - \boldsymbol{H}\boldsymbol{d})^2}{\sigma_n^2}\end{aligned} \tag{22}$$

where y_n is the n-th element of $\boldsymbol{y}$ and $\ln(\cdot)$ is the natural logarithm.

C. Characterization of Channel Matrix

To evaluate the characteristics of the estimated value of the channel matrix $\widehat{\boldsymbol{H}}$, we considered the Frobenius norm, denoted as $||\widehat{\boldsymbol{H}}||_F$, which is an index of the total received optical power of the optical array when the transmitted optical power is constant. $||\widehat{\boldsymbol{H}}||_F$ is defined by

$$||\widehat{\boldsymbol{H}}||_F = \sqrt{\sum_{n=1}^{N}\sum_{m=1}^{M} \widehat{h}_{n,m}^2} \tag{23}$$

Furthermore, the condition number is a metric measuring the relative magnitudes of the singular values of the channel matrix $\widehat{\boldsymbol{H}}$. The condition number, denoted as κ, is defined by

$$\kappa_2(\widehat{\boldsymbol{H}}) = ||\widehat{\boldsymbol{H}}||_2 \cdot ||\widehat{\boldsymbol{H}}^{-1}||_2 = \frac{\sigma_{max}(\widehat{\boldsymbol{H}})}{\sigma_{min}(\widehat{\boldsymbol{H}})} \tag{24}$$

where $\sigma_{max}(\widehat{\boldsymbol{H}})$ and $\sigma_{min}(\widehat{\boldsymbol{H}})$ indicate the maximum and minimum singular values of $\widehat{\boldsymbol{H}}$, respectively.

III. Experimental Setup and Approach

As explained earlier, in this work, we extend the application of our new optical linear transmitting array [12] with $M = 8$ transmitting elements while considering two different types of receiver configuration in an indoor environment.

Table I outlines the specifications of the different equipment used in both experiments. All the optical elements are identical and were customized for the experiments. Each element includes an infrared USHIO HE8811 LED emitting at a wavelength of 820 nm and Hamamatsu S12023-05 Si-APD with a half-value

TABLE I
SPECIFICATIONS OF THE EXPERIMENTAL APPARATUS

Transmitting signal processing unit	
CPU	PXIe-8840
FPGA	PXIe-7972
DAC	PXIe-5783
Receiving signal processing unit	
CPU	PXIe-8861
ADC	
Type	PXIe-5170
Bandwidth	100 MHz
Sampling rate	250 MSample/s
Optical element	
Type	Toyo Electric SOT-ES200 (customized for experiments)
LED	USHIO INK. HE8811
APD	Hamamatsu Photonics K.K. S12023-05
Wavelength	820 nm (IR)
Half-value angle	1°
3 dB Bandwidth	100 kHz∼40 MHz
Maximum gain frequency	500 kHz
Imaging optical device	
Focal length	80∼400 [mm]
F-number	4.5
Focus	Infinity
APD array	Hamamatsu Photonics K.K. S14137-01CR

TABLE II
SPECIFICATIONS OF C- AND I-MIMO EXPERIMENTS

Experiment environment	
Experimental location	Indoor
Conventional MIMO size	8×8
Imaging MIMO size	8×16
Element spacing (d)	17.5 cm
Optical element altitude	71 cm
Communication distance (L)	20 m−65 m
Signal parameters	
Transmission line code	Manchester code
Equalization method	Zero forcing
	Maximum likelihood
Symbol rate	25 Mbit/s ×8
Number of transmitted data bits	778240 [bits]
	38 Frames

angle of one degree. All eight elements have the same data rate of 25 Mbps, as outlined in Table II. Therefore, the maximum achieved data rate is 200 Mbps. Moreover, we considered the period K as $K = 10$.

The angle of each transmitting element was adjusted to capture the maximum of the incident light to the receiving elements

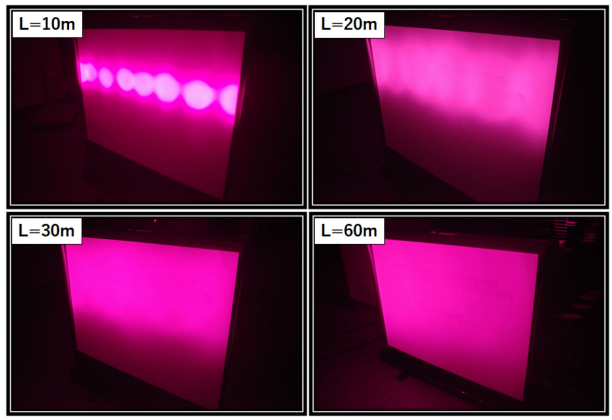

Fig. 5. Infrared photographs of the transmitted beams projected on a screen at different distances $L = 10$ m, 20 m, 30 m, and 60 m.

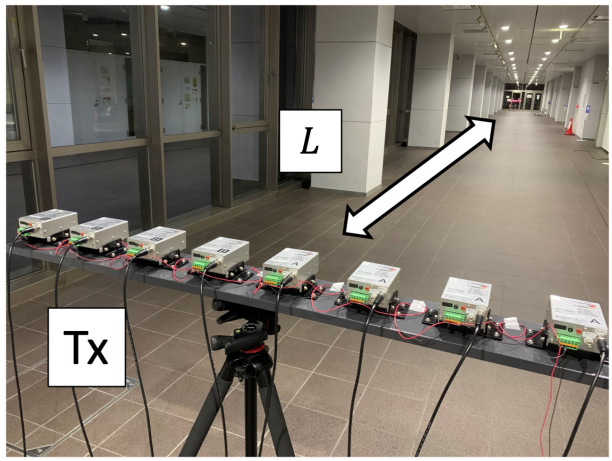

Fig. 6. View of the experiment site.

using an infrared camera PENTAX-DA with a focal length within the range (18 mm∼55 mm). The infrared photographs of the transmitted beams projected on a white screen at different transmission distances are illustrated in Fig. 5.

The c-MIMO system employs a similar one-dimensional receiving APD-based array on the receiver side. Each receiving element includes a square Fresnel lens with an aperture of 3.3 cm× 3.3 cm placed in front of a Hamamatsu S12023-05 Si APD with a light-receiving surface size of ϕ 0.5 mm. In the i-MIMO system, the imaging camera-based receiver design consists of a single optical device that includes a telephoto lens, namely Tokina ATX 840 AF II with a wide field of view within the range of [29°30'-6°8'], installed in front of the classic single-lens reflex camera, Nikon-F, with a 16-element APD array S14137-01CR array instead of a film, as shown in Fig. 3. The linear receiving array, i.e., Hamamatsu S14137-01CR, incorporates a compact 16-element Si-APD array and a transimpedance amplifier. This APD array has a light-receiving surface size/per channel that equals 0.15 × 0.43 mm. For the c-MIMO and i-MIMO systems, the APDs have the same photosensitivity of 0.5 A/W. As explained earlier, considering the implementation

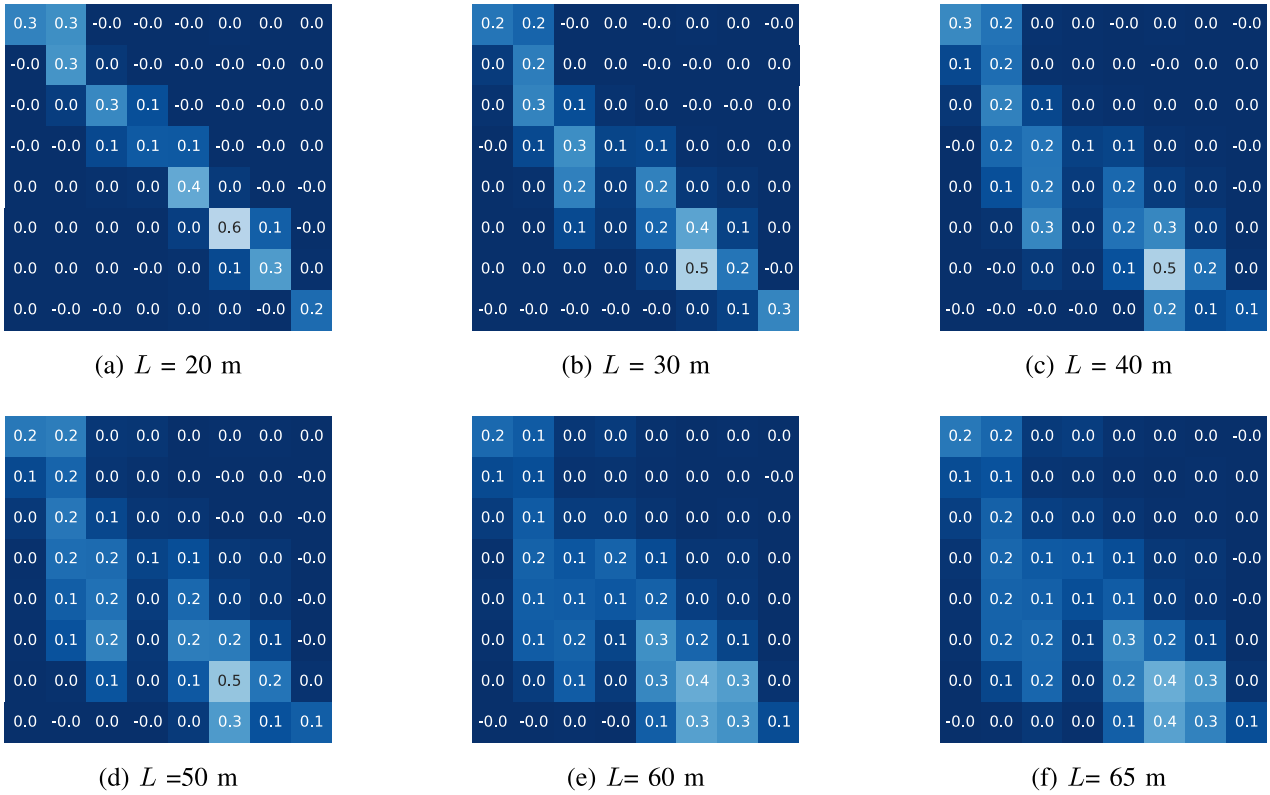

(a) L = 20 m (b) L = 30 m (c) L = 40 m

(d) L =50 m (e) L= 60 m (f) L= 65 m

Fig. 7. Normalized estimated channel matrix $\widehat{H}/||\widehat{H}||_F$ at different distances for c-MIMO system.

reasons, different APDs are used for c-MIMO and i-MIMO systems. In fact, the configuration of the i-MIMO system requires a compact APD array with multiple channels. On the other hand, the c-MIMO system includes independent optical elements that can carry on the transmission in both directions.

The experimental setup is described in Fig. 6. The spacing between two consecutive optical elements corresponds to $d =$ 17.5 cm. The transmission distance between the transmitting optical array and either the imaging receiver or linear receiving array corresponds to L such that $L = \{20$ m, 30 m, 40 m, 50 m, 60 m, 65 m$\}$ with 65 m being the limit of our experiment area.

IV. Experimental Results and Discussions

In this section, we present the performance results of both the c-MIMO and i-MIMO systems in terms of the estimated transmission channel matrix, the BER, and the condition number based on the collected data experimentally processed at the ADC offline.

A. Evaluation of Channel Matrix

For the c-MIMO system, the detection is performed considering both ZF and MLD techniques to characterize the impact of the transmission distance. The normalized estimated channel matrices, denoted as $\widehat{H}/||\widehat{H}||_F$, for the c- and i-MIMO systems at different distances ranging from 20 m to 65 m, are depicted in Fig. 7 and Fig. 8, respectively. From Fig. 7(a) and (b), it can be seen that at short distances of 20 m and 30 m, almost the matrix elements outside the main diagonal are all zero, in the case of the c-MIMO system, which means that each transmitted signal can be separated efficiently and received by the receiving element opposite to the direction of the corresponding transmitting one. On the other hand, as the transmission distance increases up to 65 m, we can notice that the performance of the c-MIMO system deteriorates since the off-diagonal components can no longer be ignored, as shown in Fig. 7(c)–(f). This is expected since the OWC systems suffer particularly from the issue of high spatial correlation in the case of c-MIMO configuration.

In the case of the i-MIMO system, the channel matrices are sparse regardless of the transmission distances, as shown in Fig. 8(a)–(f). All elements are almost zero except those expressing the path between an optical transmitting element and its corresponding receiving APD.

B. Evaluation of Bit-Error Rate

Fig. 9 illustrates the relationship between the communication distance and the BER while considering both direct detection ZF and MLD methods for the c-MIMO and ZF for i-MIMO systems. The BER is calculated for 38 data frames, including 778240 bits.

At a short distance of 20 m, the c-MIMO system ensures an error-free transmission (BER of 10^{-9}). As the distance increases to 30 m, a BER of 6×10^{-6} can be achieved in the case of the i-MIMO system combined with ZF and c-MIMO system using MLD. When the transmission distance is longer than

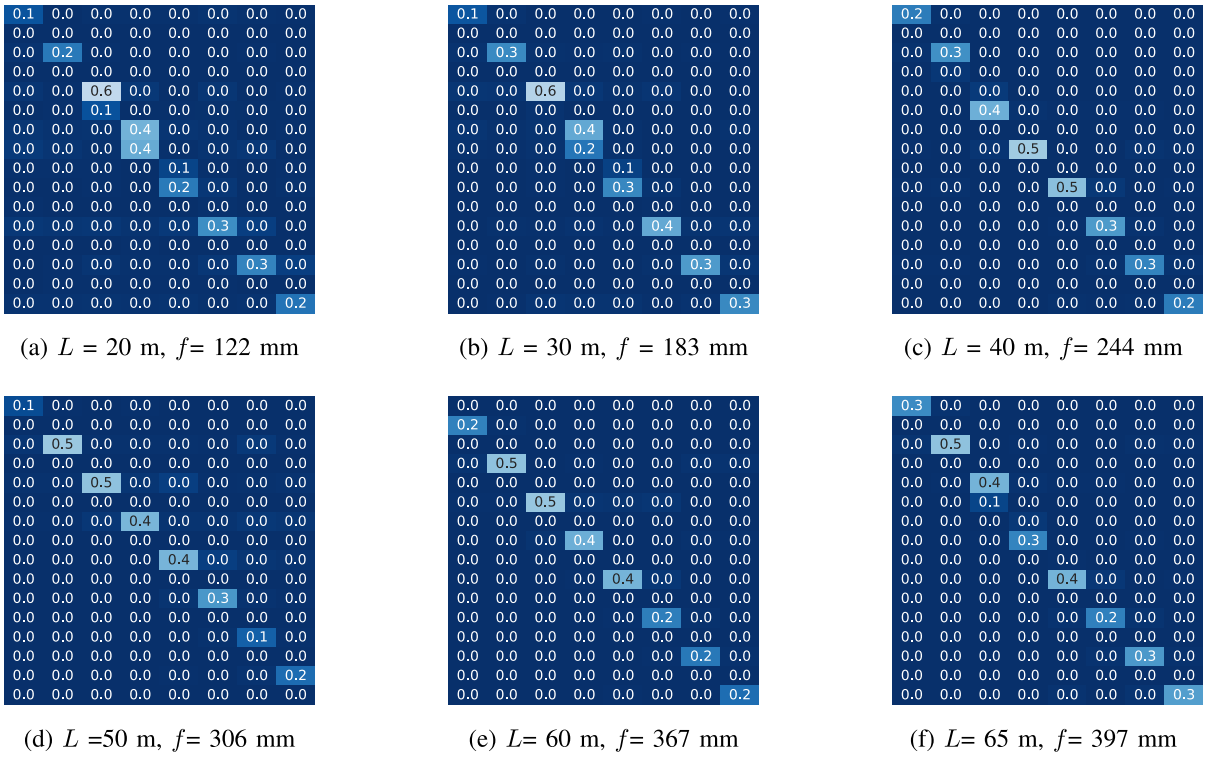

(a) L = 20 m, f= 122 mm (b) L = 30 m, f = 183 mm (c) L = 40 m, f= 244 mm

(d) L =50 m, f= 306 mm (e) L= 60 m, f= 367 mm (f) L= 65 m, f= 397 mm

Fig. 8. Normalized estimated channel matrix $\widehat{H}/||\widehat{H}||_F$ at different distances for i-MIMO system.

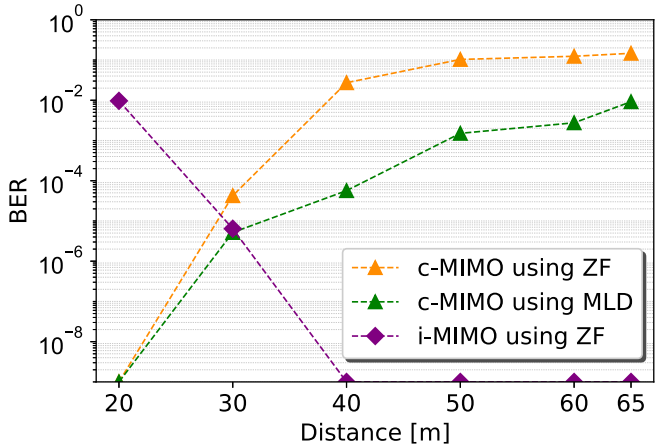

Fig. 9. BER performance in terms of transmission distance for both c-MIMO and i-MIMO systems.

40 m, the performance of the i-MIMO using ZF is noticeably improved, reaching a BER of 10^{-9}. The c-MIMO system shows a satisfactory BER as low as 5×10^{-5} at a distance of 40 m when the MLD technique is applied. An improvement of about 10^{-3} in the BER is achieved with the use of MLD rather than ZF, as expected.

In fact, for the i-MIMO system, at short distances up to 30 m, a smaller amount of the light emitted from the optical elements placed at the edge of the transmitting array, i.e., elements N1 and N8, can be caught by the receiving APD array placed within the optical device. Moreover, it is more difficult to separate the transmitted beams at short distances efficiently. This can be clearly seen Fig. 8(a) and (b) at 20 m and 30 m, respectively. On the other hand, the transmitted optical signals can still be separated in the case of the c-MIMO system at short distances up to 30 m. As shown in Fig. 7(a) and (b), the normalized estimate of the transmission matrices includes almost only non-zero diagonal elements at 20 m and 30 m, respectively. However, at longer distances exceeding 40 m, the i-MIMO system ensures an efficient separation between the different received beams thanks to the use of the optical imaging device, and an error-free transmission is possible. In the case of the c-MIMO system using the MLD technique, a BER of 1.5×10^{-3} and 9×10^{-3} is obtained at 50 m and 65 m, respectively. To the best of our knowledge, transmitting at a 200 Mbps data rate over a distance of 65 m is considered the highest data rate that could be achieved at the longest distance by indoor optical 8×8 MIMO system, using off-the-shelf LEDs and PDs.

C. *Evaluation of Condition Number*

To better understand this behavior, we take a look at the variation of the condition numbers of the estimated channel matrices at different distances up to 65 m for the c-MIMO and i-MIMO systems, as illustrated in Fig. 10. As seen from the figure, the condition number of the channel matrix increases proportionally to the communication distance. Moreover, the condition number is small when the i-MIMO system is considered, showing that the channel matrix $\boldsymbol{H}$ is well-conditioned, which concurs with the normalized estimate of the transmission matrices, including

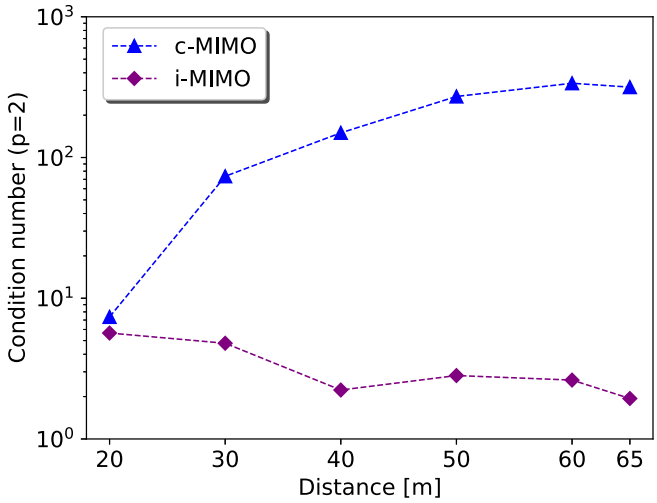

Fig. 10. Variation of the condition number in terms of the communication distance for c-MIMO and i-MIMO systems.

only non-zero diagonal elements, as shown in Fig. 8. In the case of the c-MIMO system, the condition number is large, which means that the channel matrix $\boldsymbol{H}$ is ill-conditioned.

V. Conclusion

In this paper, we considered two types of optical MIMO systems, i-MIMO, and c-MIMO designed for our experiments. Both systems employed the same linear transmitting array. The c-MIMO system used a similar linear receiving array, whereas the i-MIMO system used a customized imaging camera-based receiver design. The performance of both MIMO systems is experimentally evaluated for different transmission distances in terms of the BER and the channel matrix. Based on the obtained results, we determined the transmission specifications for each MIMO system.

Therefore, the presented analysis provides useful insights on the important constraints to consider for an efficient design of optical MIMO systems.

Acknowledgment

The authors would like to thank Prof. Takaya YAMAZATO of Nagoya University for his guidance and encouragement in carrying out this research.

References

[1] P. W. Berenguer et al., "Optical wireless MIMO experiments in an industrial environment," *IEEE J. Sel. Areas Commun.*, vol. 36, no. 1, pp. 185–193, Jan. 2018.

[2] B. Holfeld et al., "Wireless communication for factory automation: An opportunity for LTE and 5G systems," *IEEE Commun. Mag.*, vol. 54, no. 6, pp. 36–43, Jun. 2016.

[3] W. Jiang, B. Han, M. Habibi, and H. Schotten, "The road towards 6G: A comprehensive survey," *IEEE Open J. Commun. Soc.*, vol. 2, pp. 334–366, 2021.

[4] T. Fath and H. Haas, "Performance comparison of MIMO techniques for optical wireless communications in indoor environments," *IEEE Trans. Commun.*, vol. 61, no. 2, pp. 733–742, Feb. 2013.

[5] W. O. Popoola, E. Poves, and H. Haas, "Error performance of generalised space shift keying for indoor visible light communications," *IEEE Trans. Commun.*, vol. 61, no. 5, pp. 1968–1976, May 2013.

[6] A. Yesilkaya, E. Basar, F. Miramirkhani, E. Panayirci, M. Uysal, and H. Haas, "Optical MIMO-OFDM with generalized LED index modulation," *IEEE Trans. Commun.*, vol. 65, no. 8, pp. 3429–3441, Aug. 2017.

[7] Y. Wang and N. chi, "Demonstration of high-speed 2×2 non-imaging MIMO Nyquist single carrier visible light communication with frequency domain equalization," *J. Lightw. Technol.*, vol. 32, no. 11, pp. 2087–2093, Jun. 2014.

[8] C. Hsu, C. Chow, I. Lu, Y. Liu, C. Yeh, and Y. Liu, "High speed imaging 3×3 MIMO phosphor white-light LED based visible light communication system," *IEEE Photon. J.*, vol. 8, no. 6, Dec. 2016, Art. no. 7907406.

[9] L. Wei, H. Zhang, and J. Song, "Experimental demonstration of a cubic-receiver-based MIMO visible light communication system," *IEEE Photon. J.*, vol. 9, no. 1, Feb. 2017, Art. no. 7900107.

[10] A. Burton, H. L. Minh, Z. Ghassemlooy, E. Bentley, and C. Botella, "Experimental demonstration of 50-Mb/s visible light communications using 4×4 MIMO," *IEEE Photon. Technol. Lett.*, vol. 26, no. 9, pp. 945–948, May 2014.

[11] F. Corona, H. Sugiura, K. Kobayashi, H. Okada, and M. Katayama, "Experimental evaluation of an optical wireless MIMO system with baseband modulation," IEICE Tech. Rep., RCS 2018–115, vol. 118, no. 125, pp. 165–169, 2018.

[12] T. Nakamura, C. B. Naila, K. Kobayashi, H. Okada, and M. Katayama, "Experimental evaluation of indoor optical wireless MIMO systems with square and linear array constellations," *IEEE Photon. J.*, vol. 13, no. 1, Feb. 2021, Art. no. 7900612.

[13] Z. Ghassemlooy, P. Luo, and S. Zvanovec, "Optical camera communications," in *Optical Wireless Communications*. Cham, Switzerland: Springer, Aug. 2016, pp. 547–568.

[14] L. Zeng et al., "High data rate multiple input multiple output (MIMO) optical wireless communications using white LED lighting," *IEEE J. Sel. Areas Commun.*, vol. 27, no. 9, pp. 1654–1662, Dec. 2009.

[15] P. Butala, H. Elgala, and T. D. C. Little, "Performance of optical spatial modulation and spatial multiplexing with imaging receiver," in *Proc. IEEE Wireless Commun. Netw. Conf.*, 2014, pp. 394–399.

[16] T. Chen, L. Liu, B. Tu, Z. Zheng, and W. Hu, "High-spatial-diversity imaging receiver using fisheye lens for indoor MIMO VLCs," *IEEE Photon. Technol. Lett.*, vol. 26, no. 22, pp. 2260–2263, Nov. 2014.

[17] A. K. Gupta and A. Chockalingam, "Performance of MIMO modulation schemes with imaging receivers in visible light communication," *IEEE J. Lightw. Technol.*, vol. 36, no. 10, pp. 1912–1927, May 2018.

[18] A. H. Azhar, T. Tran, and D. O'Brien, "A gigabit/s indoor wireless transmission using MIMO-OFDM visible-light communications," *IEEE Photon. Technol. Lett.*, no. 2, vol. 25, pp. 171–174, Jan. 2013.

[19] B. Fahs et al., "A meter-scale 600-Mb/s 2×2 imaging MIMO OOK VLC link using commercial LEDs and Si p-n photodiode array," in *Proc. IEEE 26th Wireless Opt. Commun. Conf.*, 2017, pp. 1–6.

[20] A. Iwasa, C. Ben Naila, K. Kobayashi, H. Okada, and M. Katayama, "Experimental evaluation of an indoor long distance high speed imaging MIMO system," in *Proc. IEEE Glob. Commun. Conf.*, 2020, pp. 1–6.

[21] J. G. Proakis, *Digital Communications*, 5th ed. New York, NY, USA: McGraw-Hill, 2008.

[22] G. Strang, *Introduction to Linear Algebra*, 5th ed. Cambridge, MA, USA: Wellesley-Cambridge, 2016.